Solid-State Polymerization of Poly(ethylene terephthalate). I. Experimental Study of the Reaction Kinetics and Properties

T. Y. Kim, E. A. Lofgren, S. A. Jabarin

Polymer Institute and Department of Chemical and Environmental Engineering, University of Toledo, Toledo, Ohio 43606-3390

Received 7 March 2002; accepted 10 August 2002

ABSTRACT: The solid-state polymerization (SSP) reaction kinetics of poly(ethylene terephthalate) were investigated in connection with the initial precursor intrinsic viscosity (IV; molecular weight). Evaluations were performed with otherwise equivalent precursors melt-polymerized to IVs of 0.50, 0.56, and 0.64 dL/g. The changes in the molecular weight and other properties were monitored as functions of the reaction times at solid-state temperatures of 160–230°C. Precursors with higher initial molecular weights exhibited higher rates of SSP than those with lower initial values, as discussed in connection with the levels of crystallinity and the carboxyl and hydroxyl end-group composition. Activation energies decreased at temperatures above 200°C, and this indicated a change in the SSP reaction mechanism. At temperatures of 200–230°C, similar activation energies were required for the polymerization of all three precursors. Lower temperature polymerizations, from 160 to 200°C, required higher activation energies for all precursors, with the 0.50-IV material requirement almost twice as high as that calculated for the higher IV precursors. © 2003 Wiley Periodicals, Inc. J Appl Polym Sci 89: 197–212, 2003

Key words: solid-state polymerization; polyesters; crystallization; esterification

INTRODUCTION

Poly(ethylene terephthalate) (PET) has extensively been used in the form of staple or filament fibers and films.[1,2] The resins used for these applications are generally obtained by melt-phase polymerization to intrinsic viscosities (IVs) of 0.5–0.7 dL/g. PET has also been used for soft drink and beverage bottles, tire cord filaments, and industrial fibers. These products require a higher molecular weight than that produced by melt-phase polymerization. For the preparation of PET, which has an IV greater than 0.7 dL/g, solid-state polymerization (SSP) is generally carried out by the heating of solid, low molecular weight, melt-phase-polymerized PET below its melting point but above its glass-transition temperature (T_g). SSP of PET is not an independent process of, but rather an additional process to, melt polymerization, used when PET of a higher molecular weight is required.[3,4]

Although the melt polymerization process can produce PET of higher molecular weight, it causes many problems with respect to resin quality because of the degradation coming from long reaction times at high temperatures. It may also cause problems for polymerization equipment because of the abrupt increases in the melt viscosity as the molecular weights of the reactants increase. These problems in obtaining high molecular weight PET with a melt-phase process have been overcome by SSP.[1–4]

An important feature of SSP is that this process requires relatively simple equipment, and the reaction proceeds under relatively moderate conditions. For example, the SSP temperature range is 200–220°C, which is 60–80°C lower than that of melt-phase polymerization. SSP uses an inert purge gas or vacuum as a way to remove byproducts such as ethylene glycol (EG), water, and acetaldehyde (AA). The equilibrium of the reaction is continuously moved in the forward direction by the removal of reaction byproducts during SSP.[5,6] PET produced from melt-phase polymerization is conventionally called a precursor. The material state of the precursor is amorphous because it has been quenched by cold water after being extruded from the melt-phase polymerization reactor. PET, in its amorphous state, is thermally and dimensionally stable only up to its T_g, which is around 80°C. When heated above T_g, the polymer becomes soft and rubbery. This causes the amorphous PET pellets to stick to one another, especially at SSP reaction temperatures, which are usually above 200°C. Once PET is crystallized to some degree, the limiting point for the stiffness and rigidity of the material shifts from T_g toward its melting temperature. The melting temperature of

Correspondence to: S. A. Jabarin (sjabari@utnet.utoledo.edu).
Contract grant sponsor: PET Industrial Consortium.

PET, which generally ranges from 240 to 270°C, is much higher than its T_g and is dependent on the degree of crystallinity and the perfection of the crystalline structure.[6–9] The crystallization of the precursor before SSP is, therefore, used to avoid any sticking problems among the pellets inside the reactor.

SSP kinetic considerations

The polymerization of PET is conventionally considered to be accomplished by two reversible reactions in SSP. One is the ester-interchange reaction (or transesterification reaction):[4]

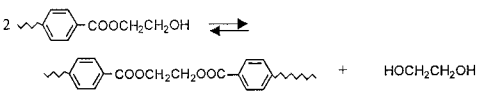

(1)

The other one is the esterification reaction:[4]

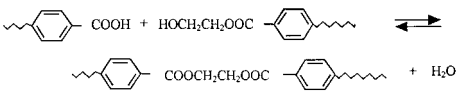

(2)

The rates of these reactions are important in determining the overall SSP rate. There are several other steps that affect the overall SSP rate and also complicate the kinetic analysis of SSP. One way to determine SSP kinetics and mechanisms is through an experimental approach. This approach can be successfully used as a way to discern the rate-determining mechanisms. Researchers[1,3] have tried to find the important mechanisms of SSP kinetics by investigating the effects of many variables on the SSP rate. From the importance of each variable, the mechanism that is acting as the rate-determining step can be identified at a certain condition of SSP. It has been found that the main polymerization reaction can be considered an equilibrium reaction in which the byproducts of EG and water are removed so that the forward reaction will be favored. The overall reaction rate depends on both chemical and physical processes. Depending on the process and operating variables, the overall SSP rate is controlled by one or more of the following steps:[3–5,10]

Step 1. Diffusion of the molecular chain end groups in the solid phase.
Step 2. Reversible chemical reactions between the molecular chain end groups.
Step 3. Diffusion of the volatile byproducts (EG, water, and AA) in the solid polymer.
Step 4. Diffusion of the volatile byproducts from the polymer surface to the inert gas.

Several considerations must be made to understand SSP kinetics. Because all the reactions take place in the solid phase, the mobility of the polymer chains is limited. If a crystalline phase is present, the segmental mobility of the molecular chains can be expected only in the amorphous region, not in the crystalline phase. This segmental mobility can be affected by material variables such as the crystallinity, the size and distribution of the crystalline phase, and the degree of copolymerization. In SSP, the mobility of the polymer chains is believed to decrease as SSP proceeds because the crystallinity increases and the crystalline structure becomes more stable during SSP. This makes the reaction rate constants decrease as SSP proceeds; this is different from the case of general chemical reactions or melt-phase reactions, in which the reaction constants remain unchanged and the reductions in the reaction rate result from diminishing concentrations of reactants. Some researchers[5,11] have used the reaction rate constants in their SSP models by extrapolating to lower temperatures with the same activation energies and frequency factors developed for melt-phase reactions. This approach produces errors for the reasons mentioned previously.

The polymerization reaction and diffusion of the reaction byproducts usually occur simultaneously. The decoupling of the byproduct diffusion from the reactions could, therefore, be an additional factor that complicates analyses of the SSP kinetics. The estimation of diffusivities of byproducts is not easily accomplished because several diffusion processes take place simultaneously as reactions occur, making the determination of the individual rate constants more complicated. Because of these difficulties, published SSP models have depended on individual experimental results. These models contain one or sometimes more than one parameter to fit the modeling results to the experimental data.[4,5,10–15]

Although the kinetic analyses based on each mechanism help to clarify what is happening during the SSP process, they are not always feasible or appropriate, especially when comparative studies of the SSP rates are performed. Rate-determining mechanisms can change according to reaction conditions[3] and are often unknown at a certain condition. For the purpose of a comparative study, it would, therefore, be helpful to obtain apparent rate constants that can be used without assumptions concerning the reaction mechanisms, rather than to use the complicated models that have been made based on assumptions about SSP mechanisms. In this manner, IVs or molecular weight data have been plotted as functions of the square root of SSP time by several researchers.[16,17] This method of plotting has often been used in kinetic analyses, in which a diffusion step is involved in the process. These plots yield apparent SSP rate constants, regardless of SSP times, which are convenient to compare, even though they do not give fundamental information about SSP kinetic mechanisms.

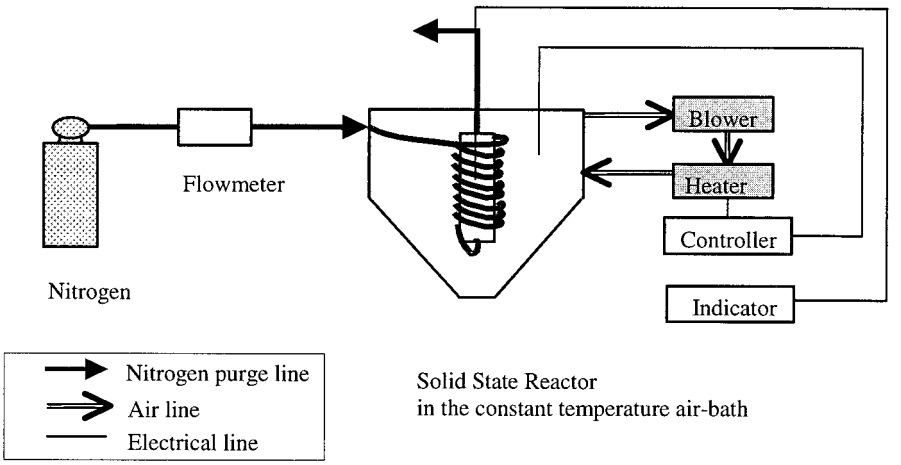

Figure 1 Schematic diagram of the bench-scale SSP system.

Many variables are involved in the SSP of PET. Among them, the precursor initial IV (IV_0) is of major importance because of its influences on SSP kinetics and other material properties. Few studies, however, have been published with respect to the effects of the precursor IV. Wu et al.[13] reported their modeling results, describing the effect of IV0 on SSP rates. We investigated in more detail how changes in IV0 affected the SSP kinetics. Another objective of this study was to monitor changes in the material properties due to SSP and to examine how SSP affected the properties related to the crystalline structure and thermal stability, especially in terms of the generation of AA and the vinyl ester groups. In this article, the first of a three-part series, kinetic studies are examined that were based on an experimental approach, and changes in some properties, such as the molecular weight, the concentrations of carboxyl end groups and hydroxyl end groups, the crystallinities, and the crystallite sizes, are documented.

EXPERIMENTAL

Bench-scale SSP system

The SSP system was composed of a reactor, preheater, nitrogen cylinder, temperature controller, and gas flowmeter, as shown in Figure 1. A dryer system, including a hopper (CH12-5, Conair, Pittsburgh, PA), a blower (VB-001SE-01, Hitachi, Ltd., Tokyo, Japan; maximum volume rate = 26.5 ft^3/min), and a heater (18159303, Conair; 240 V × 7.6 A), was used as a constant-temperature air bath. The dryer was a closed system with circulating air. The temperature of the air going to the hopper was controlled within ±1.5°C. The cylindrical stainless steel reactor, 15 cm high and 3 cm in diameter, had a 50-g resin capacity. This reactor was connected to a nitrogen purge line composed of a gas cylinder and a flowmeter. About 3 ft of the copper tubing (outside diameter ~ 0.6 cm) was coiled around the reactor from top to bottom before being connected to the inlet at the reactor bottom. The reactor and tubing around it were put inside the hopper so that they could be heated by hot air circulating inside the hopper. Nitrogen was supplied at a controlled rate for the removal of volatile products, while passing through the PET pellets. A thermocouple in the reactor was used to monitor pellet temperatures during the reactions.

SSP experiment and determination of IV

Three commercial PET precursors were made and provided by SK Chemicals (Ulsan, Korea). All of them were produced with initial diethylene glycol concentrations of 1.5 wt % with the same catalyst system, containing antimony, from a commercial continuous reactor system for PET melt polymerization. They had different IVs. Sample A had an IV of 0.50 dL/g, sample B had an IV of 0.56 dL/g, and sample C had an IV of 0.64 dL/g. The precursors had similar pellet sizes, as shown in Table I.

TABLE 1
Three Precursors and the Average Dimensions of the Pellets

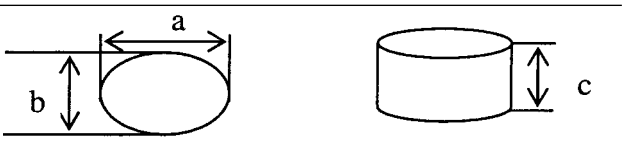

Precursors	IV (dL/g)	Pellet size (mm)		
		a	b	c
A	0.50	2.5	1.8	2.4
B	0.56	2.8	2.0	2.4
C	0.64	2.8	1.9	2.5

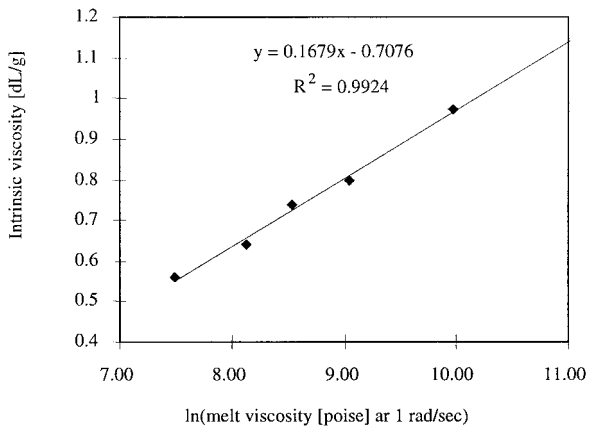

Figure 2 Standard correlation line showing the relationship between the natural logarithm of the melt viscosity at 1 rad/s and IV.

Before SSP, the precursor samples were vacuum-dried for at least 10 h at 120°C. Drying at this temperature crystallized the precursor to a level of about 30%, and this helped to prevent subsequent sticking and removed moisture, thereby preventing hydrolytic degradation. After the loaded reactor was placed in the oven, a 50-min stabilization time was required for the material to reach the desired temperature. The reaction time was counted after the material temperature was 5°C lower than the desired temperature. After each reaction was completed, the reactor was removed from the hopper while being purged with nitrogen and cooled by an external air fan. Nitrogen purging was continued until the resin had cooled to less than 80°C. The samples were then removed from the reactor and subjected to further analyses.

Several samples, over a range of melt viscosities, were selected, and the IVs were measured with a dilute solution method with 60/40 phenol/tetrachloroethane as the solvent.[16] The melt viscosities of these samples were also measured, at a temperature of 280°C and at shear rate of 1 rad/s, with a cone-and-plate rheometer. A calibration curve was made from the correlation between solution IV data and the natural logarithm of the melt viscosity, as shown in Figure 2. IV values for additional samples were calculated from melt viscosity results with this correlation line.

End-group analysis

The concentrations of carboxyl end groups in the precursors and the solid-stated samples were determined with a Fourier transform infrared (FTIR) technique. This method is discussed in articles written by Ward and coworkers[18,19] and most recently by Al-Abdul-Razzak et al.[20] This technique is based on the observation that at specific wave numbers, the areas of IR peaks are proportional to the concentrations of carboxyl end groups. Previous researchers[18–20] in this area used thin sheets of PET for measurements, but we use flattened, solid-stated pellets. In preparation for IR analyses, the pellet samples were vacuum-dried and then flattened in a potassium bromide pellet mini-press. This equipment consisted of a steel barrel and two bolts with highly polished flattened ends. Pellets were placed in the holder barrel and flattened as the two bolts were tightened against each other. After being tightened, the bolts were removed from the barrel, and IR measurements were performed with the flattened, disc-type pellet sample held in the barrel, which is also called the holder. With this pellet squeezing technique, spectral changes were recorded after various SSP conditions, as shown in Figure 3.

The method used by Ward and coworkers[18–20] utilizes peak areas (corresponding to carboxyl and hydroxyl end-group concentrations) obtained by the subtraction of the spectrum of a deuterated sample from that of an equivalent dry sample. Most of the solid-stated samples had high IVs and very low end-group concentrations. In these cases, the subtraction spectrum peaks, corresponding to carboxyl end-group concentrations, were much less clear than when higher end-group concentrations were present. Figure 4 gives examples of subtraction spectra representing a precursor with high end-group concentrations and a sample solid-stated to a high molecular weight with low end-group concentrations. To overcome this difficulty, we made several modifications to the method. The carboxyl end-group concentrations reported in these studies, therefore, resulted from absorbance height intensity measurements taken at 3268 cm−1, rather than measurements of peak areas.

The squeezed and flattened pellet samples were used directly for end-group determinations without the addition of thermal processes that would affect end-group contents. Because the samples were flattened at room temperature, they sometimes contained small voids and were of nonuniform thickness. This made it difficult to accurately measure their thickness values, which could affect the results. The normalization technique used to overcome these problems is based on the absorbance intensity at 3995 cm−1. To verify the validity of the normalization process, we conducted FTIR experiments on samples of different thicknesses that were prepared by the squeezing of one, two, and three pellets (vacuum-dried at 120°C). After the intensity at 3714 cm−1 was set as the zero point, the absorbance intensities (I_{COOH}) at 3268 and 3995 cm−1 were found to be proportional to the thickness. By the normalization of the intensity at 3268 cm−1 with the intensity at 3995 cm−1, a spectral comparison could be made independently of the thickness measurements. The normalized intensity, N_{COOH}, is defined as follows:

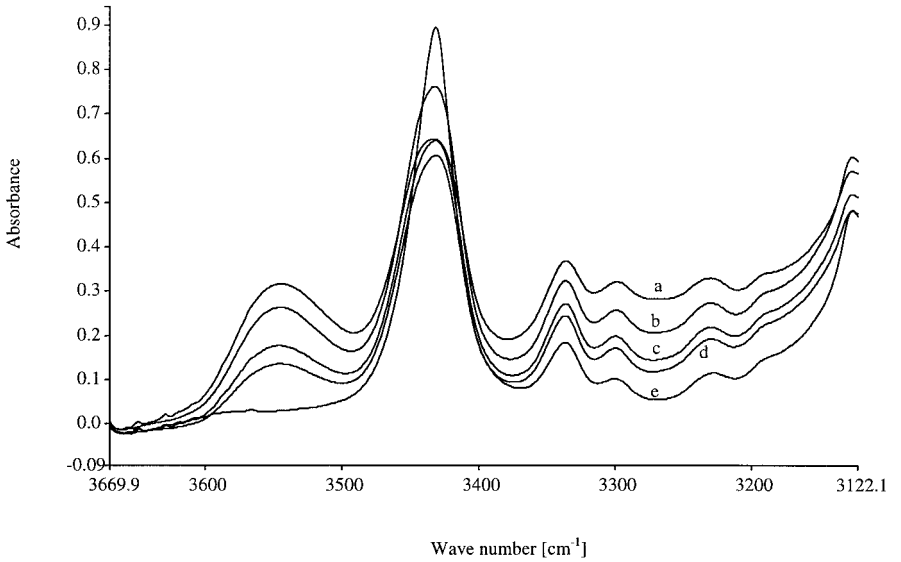

Figure 3 Absorbance FTIR spectra of (a) the precursor, (b) a sample solid-stated for 12 h at 200°C, (c) a sample solid-stated for 12 h at 220°C, (d) a sample solid-stated for 12 h at 230°C, and (e) a deuterated sample.

$$N_{\mathrm{COOH}} = \frac{I_{3268\mathrm{cm}-1} - I_{3714\mathrm{cm}-1}}{I_{3995\mathrm{cm}-1} - I_{3714\mathrm{cm}-1}} \tag{3}$$

The samples for the measurement of zero levels of carboxyl end groups were prepared by the deuteration of vacuum-dried pellets. These pellets were immersed in deuterium oxide for at least 48 h, at 50°C, under a continuous nitrogen purge, as described by others.18–20 After deuteration, each pellet was flattened and measured in the holder as previously described. The peak intensities at 3268 cm−1 were then normalized according to eq. (3). Results obtained in this manner for at least five individual deuterated pellets were found to remain constant at a normalized absorbance value of 0.47 ± 0.15. This normalized value ($N_{\mathrm{COOH}\text{-}d}$) could then be subtracted from the N_{COOH} value of each dry (nondeuterated) sample, as shown in the following equation, to give the normalized contribution of the carboxyl end groups present:

$$\begin{aligned}\Delta N_{\mathrm{COOH}} &= N_{\mathrm{COOH}} - N_{\mathrm{COOH}-d} \\ &= \left[\frac{I_{3268\mathrm{cm}-1} - I_{3714\mathrm{cm}-1}}{I_{3995\mathrm{cm}-1} - I_{3714\mathrm{cm}-1}}\right]_{\mathrm{sample}} \\ &\quad - \left[\left[\frac{I_{3268\mathrm{cm}-1} - I_{3714\mathrm{cm}-1}}{I_{3995\mathrm{cm}-1} - I_{3714\mathrm{cm}-1}}\right]\right]_{\mathrm{deuterated-sample}} \\ &\cong \left[\left[\frac{I_{3268\mathrm{cm}-1} - I_{3714\mathrm{cm}-1}}{I_{3995\mathrm{cm}-1} - I_{3714\mathrm{cm}-1}}\right]\right]_{\mathrm{sample}} - 0.47 \end{aligned} \tag{4}$$

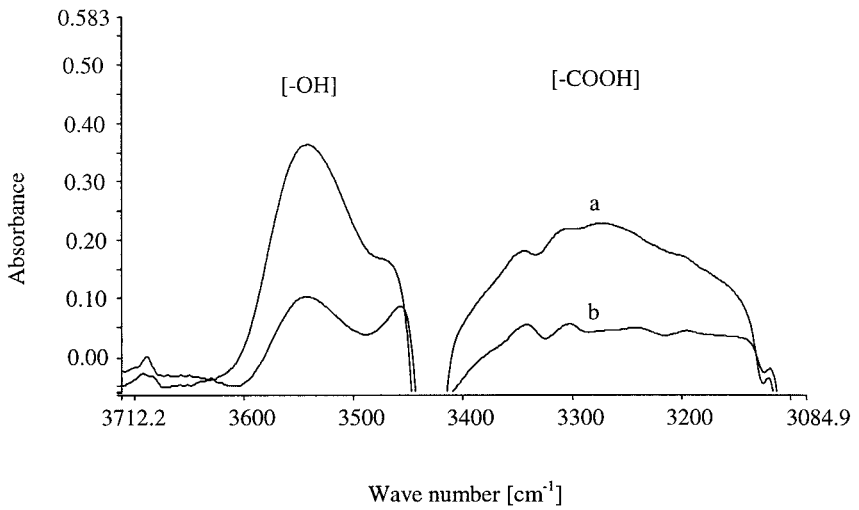

Figure 4 Difference FTIR spectra obtained after the subtraction of the spectrum of a deuterated sample from that of (a) the precursor and (b) a sample solid-stated for 12 h at 230°C.

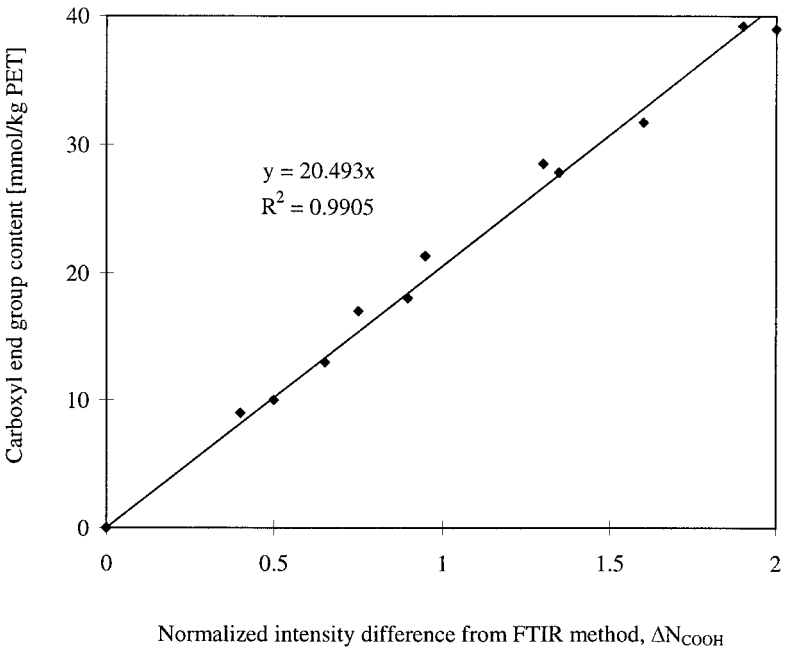

Figure 5 Calibration line showing the relationship between the normalized intensity difference obtained from the FTIR method (ΔN_{COOH}) and the carboxyl end-group content obtained from the titration method.

Selected samples, measured in the aforementioned manner, were also evaluated for carboxyl end-group concentrations with the titration method described by Jabarin and Lofgren.[16] Results obtained with the two techniques were then used to establish the correlation shown in Figure 5. Additional measurements of carboxyl end-group concentrations used this correlation and normalized IR peak height measurements.

Vinyl ester concentrations were very low in comparison with concentrations of hydroxyl ([OH]) and carboxyl ([COOH]) end groups and for simplicity have not been considered in the following calculations. If it is assumed that only [OH] and [COOH] end groups are present in PET, their concentrations can be described, in terms of the number-average molecular weight (*Mn*), according to the following relationship:[10]

$$[\mathrm{OH}] = \frac{2 \times 10^6}{M_n} - [\mathrm{COOH}] \tag{5}$$

The concentrations of hydroxyl end groups were calculated with eq. (5) with rheologically based molecular weight data and carboxyl end-group concentrations obtained with FTIR.

Other characterizations

The densities of the samples solid-stated at various conditions were measured at 25°C with a density gradient column filled with an aqueous calcium nitrate solution. The volume fraction crystallinity percentage (f) was calculated from the density values with the following relationship:

$$f = \frac{(d - d_a)}{(d_c - d_a)} \times 100 \tag{6}$$

The density for completely crystalline PET (d_c) was taken to be 1.455 g/cc,[21] and the density for amorphous PET (d_a) was taken to be 1.333 g/cc.[22]

The melting behaviors of the samples solid-stated under various conditions were monitored with a PerkinElmer (Shelton, CT) differential scanning calorimeter (DSC-7). Endotherms of dried pellet samples of about 9 mg were recorded at a heating rate of 10°C under a nitrogen atmosphere.

The sizes of the crystallites formed during SSP were determined with a wide-angle X-ray diffraction technique.[23,24] After solid-stated PET samples were ground to a particle size of less than 30 mesh, X-ray diffraction measurements were made with the powder samples at diffraction angles of 10–20°. Two peaks were observed in this range, specifically at $2\theta = 16.5°$ and $2\theta = 17.8°$, which could be called crystallites in the direction of $0\bar{1}1$ and 010, respectively. The 15–19° region in the diffracted scan was then deconvoluted into two overlapping Gaussian peaks corresponding to the two crystalline reflections, and the positions, widths, and heights of both peaks were extracted, as shown in Figure 6. The apparent crystallite size for the (010) reflection (ACS_{010}) was calculated from the peak position and the full width at half-height with the Scherrer equation:[23,24]

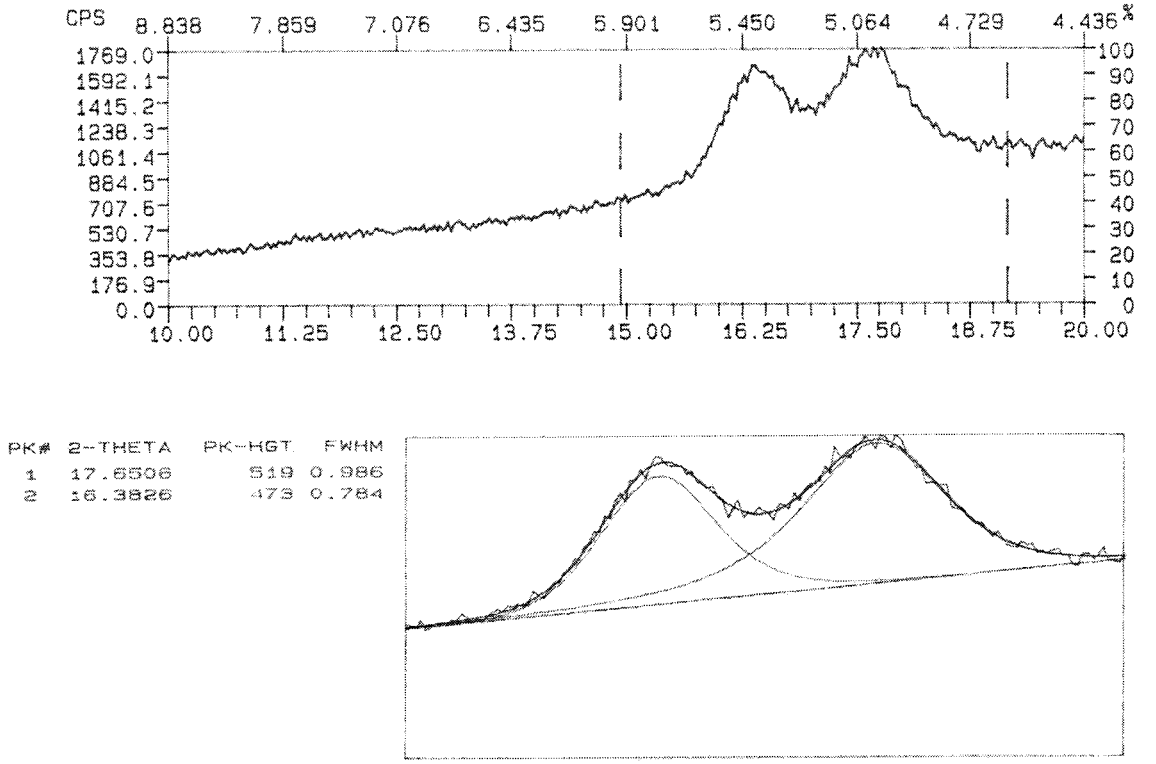

Figure 6 Deconvoluted peaks obtained for the solid-stated PET with wide-angle X-ray diffraction.

$$ACS_{010} = \frac{\kappa\lambda}{\beta_{010} \cos \theta_{010}} \quad (7)$$

where ACS_{010} is the mean dimension of the crystal in the direction normal to the plane 010, κ is assumed to be 1, λ is the wavelength of the X-ray used, β is the full width at half-height of the profile (rad), and θ is the diffracted angle. Similar calculations were performed for the $0\bar{1}1$ plane.

RESULTS AND DISCUSSION

A series of SSP experiments were conducted with three precursors with different IVs (0.50, 0.56, and 0.64 dL/g) at temperatures ranging from 160 to 230°C and for reaction times of 4, 8, and 12 h after the material temperatures were 5°C below the desired temperature. The melt viscosities of the samples were measured and the IVs were calculated with the correlation given in Figure 2. The *Mn* values were then calculated from the converted IV data with the following relationship:[16]

$$IV = 7.5 \times 10^{-4} M_n^{0.68} \quad (8)$$

where *Mn* is the initial number-average molecular weight. Changes in the IV according to the time, temperature, and precursor IV are summarized in Table II. Figure 7 shows the increase in *Mn* as a function of the square root of the SSP reaction time for precursor B (IV0 = 0.56 dL/g). Most of the data fit linearly against the square root of time, as noted in some previous

TABLE II
IV Changes During SSP According to Time, Temperature, and Precursor IV

Precursors	Temperature (°C)	IV (dL/g) 0 h	4 h	8 h	12 h
A	160	0.50	—	—	0.51
	180		—	0.53	0.56
	190		0.53	0.56	0.61
	200		0.60	0.67	0.73
	210		0.66	0.76	0.82
	220		0.74	0.82	0.94
	230		0.85	0.99	1.10
B	160	0.56	—	0.58	0.59
	180		0.57	0.63	0.65
	190		0.63	0.65	0.72
	200		0.69	0.75	0.78
	210		0.73	0.82	0.88
	220		0.81	0.92	0.96
	230		0.93	1.07	
C	160	0.64	—	—	0.67
	180		—	0.71	0.75
	190		0.71	0.78	0.82
	200		0.78	0.84	0.88
	210		0.82	0.93	0.98
	220		0.92	1.02	1.11
	230		1.02	1.15	

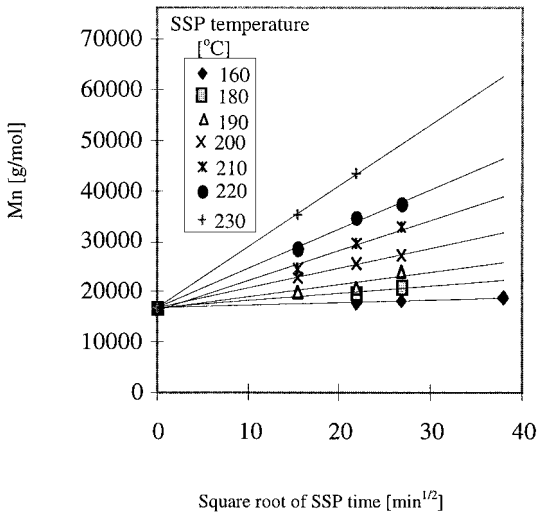

Figure 7 *Mn* as a function of the square root of the SSP time for precursor B with IV_0 = 0.56 dL/g.

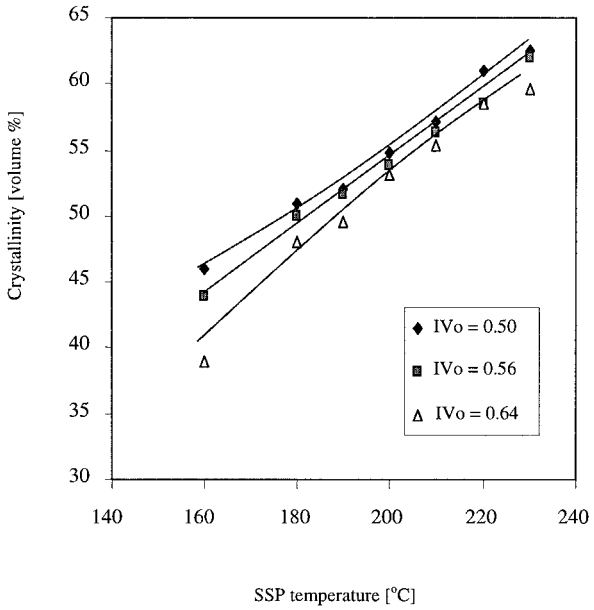

Figure 8 Change in the crystallinity as a function of the SSP temperature for samples solid-stated for 12 h from precursors with different IV_0's.

studies.[16,17] The other cases of precursors A (IV_0 = 0.50 dL/g) and C (IV_0 = 0.64 dL/g) also exhibit similar behavior. The slope of each line gives the apparent rate constant (g/mol/min$^{1/2}$) at each temperature, as shown in Table III. It was found that, as the precursor IV increased, the rate constants (k) also increased.

Wu et al.[13] and Buxbaum[25] mentioned this precursor IV effect on the SSP rate in their kinetic studies. They explained this by the negative effect of crystallinity, which means that, as the precursor IV decreases, crystallinity increases and the diffusion rate of byproducts decreases accordingly. It was also confirmed, as shown in Figure 8, that the crystallinity of a sample tends to be lower as the precursor IV increases. The effect of crystallinity on the SSP rate, however, does not appear to be straightforward. There are some differing views about this. Mallon and Ray[11] used an assumption that all the end groups exist only in the amorphous regions of semicrystalline PET. According to this assumption, if PET pellets are highly crystallized, the effective concentrations of end groups increase because of the concentration effect during crystallization. Medellin-Rodriguez et al.[26] reported that high crystallinity sometimes favored high SSP rates for PET samples that were specially prepared by precipitation in a solvent to obtain high surface areas in the precursors. These contrary effects of crystallinity can be understood with respect to the SSP kinetic mechanisms. As the SSP mechanism becomes more byproduct-diffusion-limiting, high crystallinity reduces the SSP rate by giving more resistance to mass transfer. If, however, SSP is more controlled by chemical reactions, high crystallinity can increase the SSP rate because of the effect of concentrating end groups in the amorphous region. In this experiment, pellet samples, the dimensions of which are shown in Table I, were used as precursors. For the pellet samples, crystallinity increased significantly within the first few hours of SSP and then stabilized, showing only very small increases with increased reaction time.

During the most initial stages of SSP, the polymerization reaction is thought to occur primarily near the pellet surface. At this time, byproduct diffusion is very rapid and, therefore, not inhibited by crystallinity, which can also increase the chemical reaction rate by increasing the end-group concentration. As the SSP process continues, however, end-group concentrations at the pellet surface are depleted and the SSP reactions proceed at greater depths within the pellet. As this occurs, byproduct diffusion becomes increasingly important in terms of the SSP rate. For pellet samples used for these experiments, the greater resistance to byproduct diffusion, resulting from higher levels of crystallinity, is considered to act as a negative factor that retards the SSP rate.

TABLE III
Comparison of Apparent Rate Constants

SSP temperature (°C)	k (g/mol/min$^{1/2}$)		
	IV_0 = 0.50	IV_0 = 0.56	IV_0 = 0.64
160	10	54	76
180	79	151	159
190	151	245	331
200	381	395	457
210	561	596	674
220	769	783	941
230	1138	1210	1286

TABLE IV
Change of the Molar Concentration of Chain End Groups as a Function of SSP Time and Temperature for Each Precursor

Precursor (IV)	Temperature (°C)	–OH end group (mmol/kg of PET)				–COOH end group (mmol/kg of PET)				[–COOH]/[–OH] (mol %)			
		0 h	4 h	8 h	12 h	0 h	4 h	8 h	12 h	0 h	4 h	8 h	12 h
A (0.50)	180	107	—	—	91	32	—	—	28	30	—	—	31
	190	107	—	91	82	32	—	28	25	30	—	31	30
	200	107	82	67	59	32	26	24	20	30	32	36	34
	210	107	70	57	52	32	23	19	16	30	33	33	31
	220	107	59	54	50	32	20	14	9	30	34	26	18
	230	107	49	43	39	32	15	9	6	30	31	21	15
B (0.56)	180	78	—	—	60	39	—	—	36	50	—	—	60
	190	78	—	64	53	39	—	33	30	50	—	52	57
	200	78	55	49	47	39	33	28	27	50	60	57	57
	210	78	52	—	41	39	30	26	21	50	58	—	51
	220	78	44	—	36	39	26	21	17	50	59	—	47
	230	78	36	33	—	39	19	13	8	50	53	39	—
C (0.64)	180	58	—	—	43	41	—	—	34	71	—	—	79
	190	58	—	41	37	41	—	34	32	71	—	83	86
	200	58	40	38	35	41	33	29	27	71	83	76	77
	210	58	36	31	30	41	31	26	22	71	86	84	73
	220	58	31	28	26	41	27	22	18	71	87	79	69
	230	58	29	25	—	41	23	16	13	71	79	64	—

Another reason that the SSP rate increases with increasing precursor IV can be found in the ratio of end groups ([—COOH]/[—OH]). This is also closely related to byproduct diffusion mechanisms. There is a general trend that a precursor has a lower concentration of carboxyl end groups when that precursor has a lower IV. This is often related to the conditions of melt-phase polymerization, such as lower reaction temperatures or shorter residence times. Table IV lists the results of end-group analysis after SSP at various conditions. As the precursor IV increased, the carboxyl concentration also increased. The molar ratios of carboxyl end groups to hydroxyl end groups showed the same trend, with the ratios increasing as the precursor IV increased.

As can be seen in Table IV, differences in the carboxyl concentrations and carboxyl-to-hydroxyl ratios, present among the three precursors, continued to be appear throughout the SSP process. PET resins with the same IV had equivalent total end-group concentrations; however, the ratios of carboxyl end groups to hydroxyl end groups depended on the precursor IV_0. Resins with lower precursor IV_0's (lower initial carboxyl concentrations and higher hydroxyl concentrations) also had lower carboxyl and higher hydroxyl end-group concentrations than those prepared from precursors with higher IV values and higher carboxyl concentrations and ratios. For example, resins solid-stated from each precursor to final IV values of 0.82 dL/g exhibited carboxyl concentrations of about 15, 26, and 31 mmol/kg of PET for precursors A (IV = 0.50), B (IV = 0.56), and C (IV = 0.64), respectively.

There are two main reactions responsible for the polymerization of PET. One is the ester-interchange reaction , in which 2 mol of hydroxyl end groups react and give EG as a byproduct. The other is the esterification reaction , in which a reaction takes place between a hydroxyl end group and a carboxyl end group, with water formed as a byproduct. Water is different from EG in terms of the molecular size, volatility, and rate of diffusion in the solid PET pellet. This implies that, if the SSP reaction is under byproduct diffusion control (which is often the case), the esterification reaction is advantageous in comparison with the ester-interchange reaction because the diffusion rate of water is faster than that of EG. This effect can become more significant when the SSP temperature is lower than 197.6°C (the boiling point of EG) because the ester-interchange reaction cannot easily proceed on account of the lower volatility of EG at temperatures lower than its boiling point. This illustrates one reason that precursor A, which had very low contents of carboxyl end groups, showed very low SSP rates at temperatures lower than 200°C in comparison with the other precursors.

The previous discussion also implies that there must be an optimum molar ratio of carboxyl end groups to hydroxyl end groups at which the sums of the rates of the esterification reactions and the ester-interchange reactions can be maximized. Wu et al.[13] reported a simulation of such results, stating that the SSP rate was affected by the molar ratio of the two end groups and that the maximum SSP rate could be obtained when the [—COOH]/[—OH] ratios were 0.5–

TABLE V
Frequency Factor (A) and Activation Energy (E_a)

Precursor	Low temperatures (160–200°C) A ($g/mol/min^{1/2}$)	Low temperatures (160–200°C) E_a (kcal/mol)	High temperatures (200–230°C) A ($g/mol/min^{1/2}$)	High temperatures (200–230°C) E_a (kcal/mol)
A (IV_0-0.50)	3.5×10^{19}	35	1.2×10^{10}	16
B (IV_0-0.56)	1.2×10^{12}	20	1.5×10^{10}	16
C (IV_0-0.64)	3.0×10^{11}	19	6.4×10^{9}	15

0.8, depending on the SSP temperatures. Duh[27] also reported that, after SSP experiments with precursors with IV = 0.45 dL/g (including 5 ppm of a titanium catalyst), carboxyl end-group contents played an important role in SSP kinetics, and the optimum ratio of [—COOH]/[—OH] was found to be 0.33–0.67, depending on ΔIV and the pellet size. He also pointed out that the optimum [—COOH]/[—OH] ratio for the fastest SSP rate increased as SSP proceeded under more control of byproduct diffusion. The results of our work agree with these past reports because the SSP rates increased as the [—COOH]/[—OH] ratios increased from 0.3 to 0.7.

The changing behavior of the molar ratio during SSP was also observed to be dependent on the precursor used. The [—COOH]/[—OH] molar ratios in precursors B (IV_0 = 0.56) and C (IV_0 = 0.64) were maintained above some level. For precursor A (IV_0 = 0.50), this ratio dropped from 30 to about 15 mol %, depending on the SSP conditions. This result offers a reason that precursor A (IV_0 = 0.50) showed lower SSP rates than the other two precursors. A lower [COOH]/[OH] molar ratio caused precursor A (IV_0 = 0.50) to be depleted of carboxyl end groups earlier than the other precursors. The earlier depletion of carboxyl end groups for precursor A caused the SSP process to slow down because it depended more on the ester-interchange reaction, in which byproduct diffusion was relatively more difficult.

The activation energy (Ea) and frequency factor (A) values, given in Table V, were determined from the slopes and intercepts of Arrhenius plots (Fig. 9) according the following relationship,[16] in which values for k are the apparent rate constants given in Table 3:

$$k = Ae^{\left(\frac{-E_a}{RT}\right)}$$

$$\ln k = \ln A + \left(\frac{-E_a}{RT}\right) \quad (9)$$

The changes in the slope, as shown in Figure 9, were observed according to the temperature region. This slope change is most clear for precursor A (IV_0 = 0.50) and indicates that a change in the SSP mechanism occurred as the temperature exceeded 200°C. When the temperature was higher than 200°C, activation energies for the three precursors were similar at 15–16 kcal/mol (63–67 kJ/mol). When the SSP reaction temperature was lower than 200°C, activation energies increased to 19–20 kcal/mol (80–84 kJ/mol) for precursors B and C (IV_0 = 0.56 and IV_0 = 0.64, respectively). For precursor A (IV_0 = 0.50), the activation energy significantly increased to 35 kcal/mol (146 kJ/mol). The frequency factors and activation energies increased as the precursor IV decreased in the low-temperature region of 160–200°C. In the high-temperature region of 200–230°C, however, similar values for the frequency factor and the activation energy were shown for all three precursors.

It is generally known that byproduct diffusion is the rate-controlling step as the SSP temperatures increase, whereas the chemical reaction is the rate-controlling mechanism when the temperatures are low.[3–5] The rate of chemical reaction can be affected by the diffusion rate of chain end groups because of its effect on their mobility. Previous studies on the SSP mechanism reported activation energies for the byproduct diffusion of 4–5 kcal/mol (17–21 kJ/mol)[10] and activation

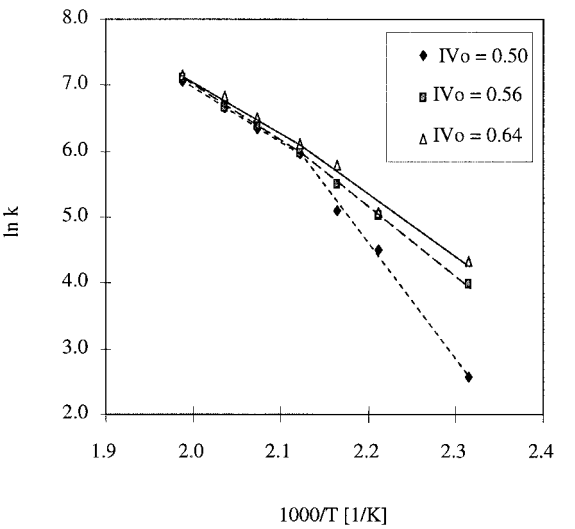

Figure 9 Arrhenius plot for the SSP of precursors with different IV_0's.

TABLE VI
Activation Energy (E_a) and Entropy Change (ΔS) for Each Step in SSP of PET, reported in the literature

SSP mechanism	E_a (kcal/mol)	E_a Reference no.	ΔS (cal/mol/K)	ΔS Reference no.
End-group diffusion	13–15	10,14	—	—
Chemical reaction	17–23	10,11,14,28	−37—−41	28
Byproduct diffusion	4–5	10	—	—

energies for the chemical reaction, which is the ester-interchange reaction or the esterification reaction, of 17–23 kcal/mol (71–96 kJ/mol).[10,11,14,28] The activation energies for the diffusion of chain end groups were reported to be 13–15 kcal/mol (54–63 kJ/mol).[10,14] Comparing the observed values in Table V with the literature values in Table VI, we observe that several factors are acting together as rate-determining steps. It is important to notice that much higher activation energies, 15–16 kcal/mol (63–67 kJ/mol), than the activation energies of byproduct diffusion, 4–5 kcal/mol (17–21 kJ/mol), were observed in the high-temperature region (200–230°C). Considering that many studies[1–4] on SSP kinetics have mentioned that the byproduct diffusion step must be a rate-determining mechanism in the high-temperature region, we now suggest that the byproduct diffusion step and the diffusion of chain end groups act together as rate-determining mechanisms. Possible rate-determining mechanisms are proposed in Table VII through a comparison of the observed apparent activation energies and the activation energies reported for each mechanism.

The entropy change (ΔS) can be calculated from the following relationship for the reaction kinetics:[29]

$$A = \frac{k_B T}{h} e^{\left(\frac{\Delta S}{R}\right)} \qquad (10)$$

$$\Delta S = R \ln\left(\frac{Ah}{k_B T}\right)$$

where A is the frequency factor from the Arrhenius equation; h is Plank's constant, which is 6.62×10^{-27} erg; k_B is Boltzmann's constant, which is 1.38×10^{-16} erg/K; and R is the gas constant, which is 1.987 cal/mol/K. The frequency factors in Table V cannot directly be used for eq. (10) because they were obtained by the plotting of molecular weight values against the square root of time and, therefore, have different units. The ratio M_n/M_{n0} can be plotted against the SSP time for precursor B, as shown in Figure 10. These data fit well only at low temperatures, especially those lower than 200°C. At higher temperatures, the data do not fit on the straight line, indicating that diffusion processes affect SSP kinetics so that the reactions become more reversible. Similar behaviors were observed for precursors A and C. The slopes of the fitted lines give the apparent rate constants, which are summarized in Table VIII. As shown in Figure 11, an Arrhenius plot can be made from these apparent rate constant values and SSP temperatures.

TABLE VII
Proposed Rate-Determining Mechanisms for Various SSP Conditions

Precursor	Low-temperature region: 160–200°C	High-temperature region: 200–230°C
A (IV_0-0.50)	End-group diffusion (≈13) + chemical reaction (≈20)	End-group diffusion (≈13) + by product diffusion (≈4)
B (IV_0-0.56)	Chemical reaction (≈20)	End-group diffusion (≈13) + by product diffusion (≈4)
C (IV_0-0.64)	Chemical reaction (≈20)	End-group diffusion (≈13) + by product diffusion (≈4)

The numbers in parentheses denote approximated values of the activation energies in kcal/mol/K for each mechanism.

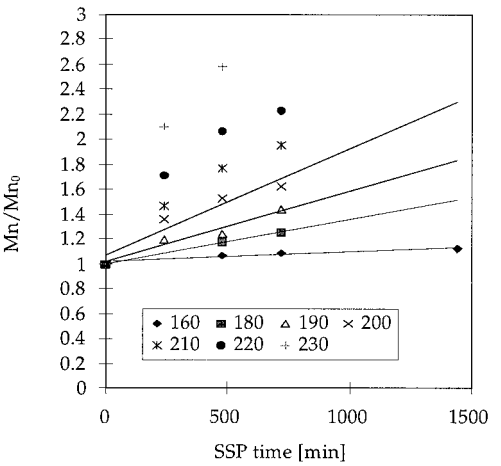

Figure 10 Plot of M_n/M_{n0} as a function of SSP time for the precursor with IV_0 = 0.56 [the numbers in the legend are SSP temperatures (°C)].

TABLE VIII
Rate Constants for the Low-Temperature Data

Temperature (°C)	k (s^{-1})		
	$IV_0 = 0.50$	$IV_0 = 0.56$	$IV_0 = 0.64$
160	3.3×10^{-7}	1.3×10^{-6}	1.7×10^{-6}
180	3.3×10^{-6}	6.7×10^{-6}	6.7×10^{-6}
190	6.7×10^{-6}	1.0×10^{-5}	1.0×10^{-5}
200	1.7×10^{-5}	1.5×10^{-5}	1.3×10^{-5}

TABLE IX
Activation Energies (E_a's), Frequency Factors (As), and Entropy Changes (ΔS's) for the Low-Temperature Data

Precursors	E_a (kcal/mol)	A (s^{-1})	ΔS (cal/mol/K)
$IV_0 = 0.50$	40	7.0×10^{13}	5
$IV_0 = 0.56$	25	9.0×10^{6}	−27
$IV_0 = 0.64$	22	2.3×10^{5}	−34

The activation energies and the frequency factors can be obtained from the slope and the intercept in an Arrhenius plot. Activation energies and entropy changes were calculated for three precursors, as shown in Table IX. Similar but slightly higher activation energies [40, 25, and 22 kcal/mol (167, 105, and 92 kJ/mol)] were obtained for each precursor than when the data were plotted against the square root of time; which had yielded activation energies of 35, 20, and 19 kcal/mol (146, 84, and 80 kJ/mol) from Table V. The differences in the activation energy can be related to the fact that kinetic behaviors digress from linearity as the SSP temperature increases. The application of a linear kinetic analysis to data at 200°C can be one cause for the differences in the activation energies obtained with the two methods.

As the precursor IV increased (0.50, 0.56, and 0.64 dL/g), the entropy decreased [5, −27, and −34 cal/mol/K (21, −113, and −142 J/mol/K), respectively]. According to transition state theory, the activation energy indicates the energy barrier between the reactant state and the transition state, and the entropy can be related to the degree of order in the transition state configuration in the reaction path. Considering these results, we can say that, as the precursor IV increased from 0.50 to 0.64 dL/g, the transition state in the reaction path had lower energy states with more ordered configurations.

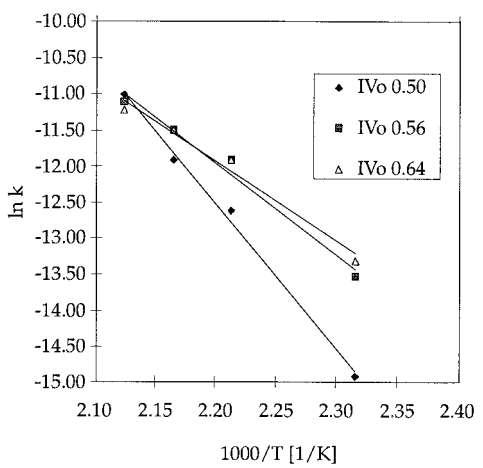

Figure 11 Arrhenius plot for the low-temperature SSP data.

The crystallite sizes in the directions of $0\bar{1}1$ and 010 were determined with a wide-angle X-ray diffraction technique. Figures 12 and 13 show the changes in the crystallite size as functions of the SSP temperatures. All the samples were solid-stated for 12 h. The crystallite sizes increased as the SSP temperatures increased. Comparing the results for the crystallites in directions $0\bar{1}1$ and 010, we find that the sizes of crystallites in the direction of $01\bar{0}$ were always larger than those in the direction of $0\bar{1}1$. These data, however, show no systematic dependence on the precursor IV. The crystallite is considered to be a unit structure in the crystalline phase that constitutes a part in the lamellae structure. As is known, PET crystallization proceeds through the formation of lamellae and spherulites. When a PET molecule is supplied with enough thermal energy to crystallize, the molecular chains tend to fold. This folded structure, called a lamella, then grows in a radial direction from a nucleus, forming a spherelike structure called a spherulite. The results indicate that the size of a unit structure is strongly dependent on the SSP temperature, but it appears to be independent of the molecular weight of the polymer. Figures 14 and 15 show the changes in the crystallite size in the direction of $0\bar{1}1$ and 010 according to the SSP time for the samples solid-stated at 220°C. The data obtained after SSP for 4, 8, and 12 h

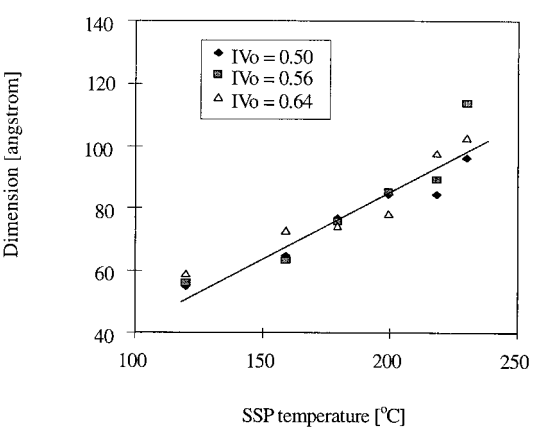

Figure 12 Crystallite size in the $0\bar{1}1$ direction according to the SSP temperature. The data at 120°C are for the precursors after crystallization at 120°C overnight before SSP. The other data are for the samples solid-stated for 12 h at the indicated temperatures.

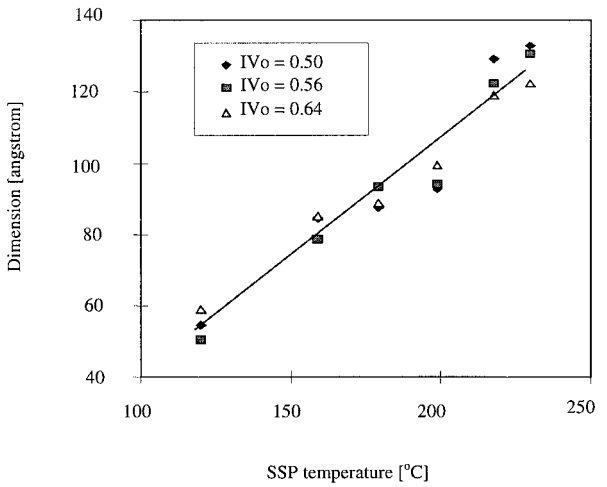

Figure 13 Crystallite size in the 010 direction according to the SSP temperature. The data at 120°C are for the precursors after crystallization at 120°C overnight before SSP. The other data are for the samples solid-stated for 12 h at the indicated temperatures.

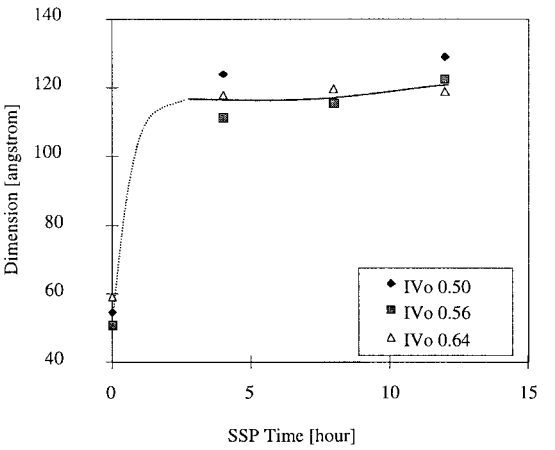

Figure 15 Crystallite size in the 010 direction according to the SSP time. The initial data at 0 h are for the precursors after crystallization at 120°C overnight before SSP. The other data are for the samples solid-stated at 220°C.

are almost the same, indicating that the crystallite size increased during the initial time of SSP, after which it stabilized. This behavior is typical of crystal growth in a polymer. After the first stage, during which its growth rate is relatively high, the growth rate becomes low, and structures stabilize in the secondary stage.

The melting behaviors of the solid-stated samples were recorded with differential scanning calorimetry (DSC). All the endotherms of the samples solid-stated at low temperatures showed double peaks, including a premelting peak of small area. The positions and areas of the first peaks were affected by the SSP conditions (temperature and time). As the SSP temperatures and times increased, the positions (or temperatures) of the first peaks shifted toward the higher temperature regions, with their areas increasing. The second peaks, however, occurred at a constant temperature with their areas decreasing (Fig. 16). Researchers[7–9] have described these phenomena and explained that they result from the incomplete crystalline structures formed during crystallization under nonideal conditions and the recrystallization of these imperfect structures during DSC scans. The first peak (premelting peak) can then be attributed to the melting peak of the incomplete structures that already existed in the pellet before DSC scanning. The second peak (main melting peak) can be assigned to the melting peak of the relatively complete structures that partly melted and recrystallized during the DSC scanning. As the SSP temperatures increased, the first peaks shifted toward the higher temperature region and, finally, merged with the second peaks. After merging, the merged single peak shifted to higher temperatures as the SSP temperatures increased.

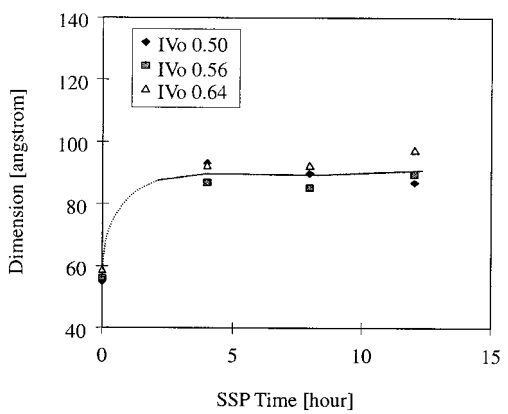

Figure 14 Crystallite size in the $0\bar{1}1$ direction according to the SSP time. The initial data at 0 h are for the precursors after crystallization at 120°C overnight before SSP. The other data are for the samples solid-stated at 220°C.

Figure 17 shows the changes in the temperatures of the first and second melting peaks. In practical consideration of the SSP process, the first premelting peaks contain important information about SSP operations. This information can help us to determine the upper limit of the SSP temperature that can be used without sticking problems occurring among pellets. Materials crystallized at higher temperatures are generally stable at higher temperatures without sticking problems. This is also the reason that a crystallization process is required before the main SSP process. After the crystallization process, pellets become more dimensionally stable during the SSP process. The temperature in the crystallization process determines the upper limit of the operating temperatures in the SSP process. The second melting peaks (or main melting peaks) contain important information with respect to the processing temperature that should be used during injection- (or extrusion-) molding processes. The molding temperature must be increased accordingly

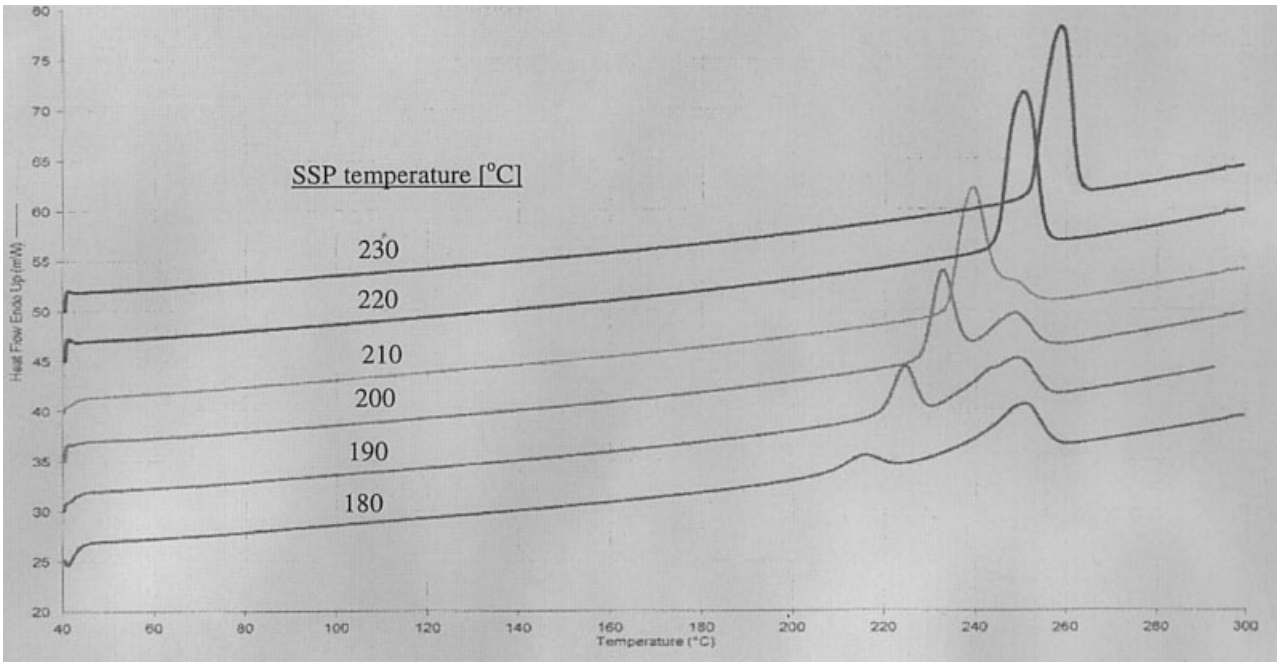

Figure 16 Melting endotherms for the PET samples solid-stated for 12 h at different temperatures from the precursors with IV = 0.50. The DSC scanning rate was 10°C/min.

as the melting temperature of the material increases. It is also known that employing higher temperatures in the molding process can cause degradation in some properties, resulting in increased AA generation, color changes, and reductions in molecular weight.[25,30,31] Figure 17 indicates that in terms of material properties, it is detrimental to increase the SSP temperature too high because this increases the melting temperature of the resin and, therefore, the operating temperature required in the injection- (or extrusion-) molding process. Some polyester applications, such as those for tire cord and high-tenacity fibers, require very high molecular weight polymers. In these cases, solid-stating at higher temperatures may be suitable, despite the resulting increases in the melting temperatures and processing requirements.

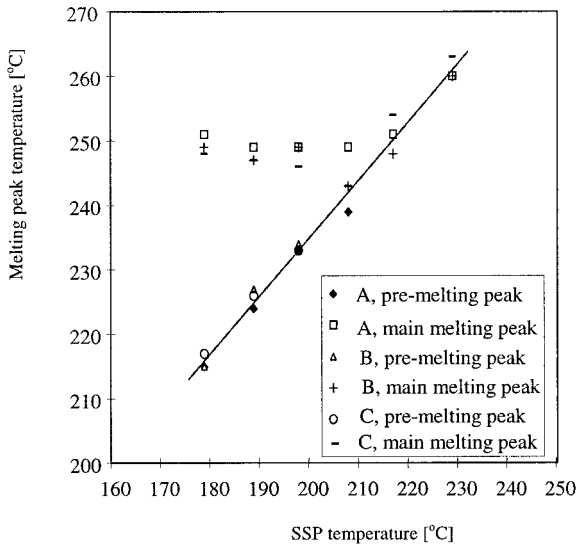

Figure 17 Melting peak temperatures as functions of SSP temperatures for different precursors: (A) $IV_0 = 0.50$, (B) $IV_0 = 0.56$, and (C) $IV_0 = 0.64$.

The area of the DSC endotherm peak can be used as another way of measuring the crystallinity percentage (x) in terms of the following equation:[6]

$$x = \frac{\Delta H}{\Delta H_0} \times 100 \tag{11}$$

where ΔH is the heat of fusion for the samples and ΔH_0 is taken as the heat of fusion for totally crystalline PET. In this case, 28.1 cal/g (117.6 J/g) was used as ΔH_0.[7]

The results give trends similar to those obtained with the density method . An interesting correlation was observed between the IV and the crystallinity calculated from DSC, as shown in Figure 18. This correlation seems to hold regardless of SSP conditions such as the temperature and time and indicates that the crystallinity percentage from the DSC scan is related to both the final IV and precursor IV. Three distinct sets of data can be seen, with levels of crystallinity at a given IV always higher for resins prepared from lower IV precursors.

CONCLUSIONS

PET precursors of three different IV_0 values were solid-state-polymerized at temperatures from 160 to

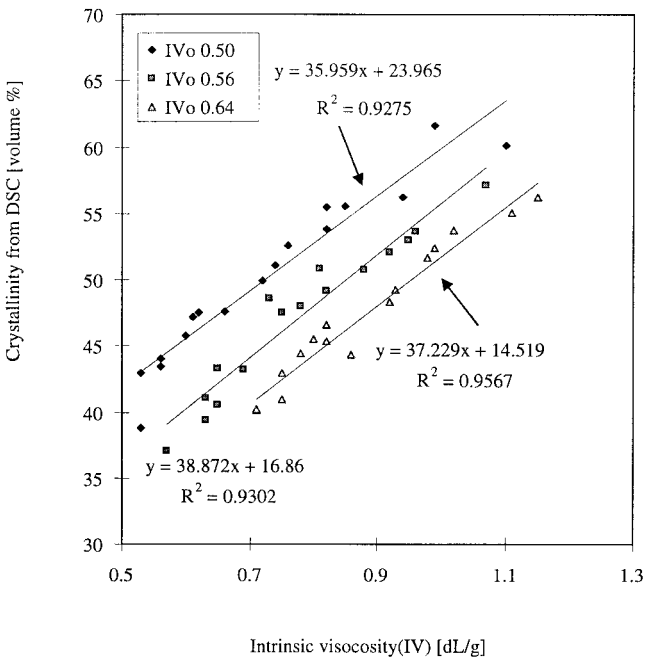

Figure 18 Correlations between crystallinity values from DSC melting endotherms and the final IVs of resins solid-stated from precursors with different IV_0 values.

230°C. The changes in the molecular weights and various other material properties were monitored as functions of the time and temperature of SSP. The kinetics of SSP were dependent on the precursor IV_0, with faster rates observed for samples with higher IV_0 values.

Analyses of carboxyl and hydroxyl end-group concentrations and their concentration ratios revealed that the SSP reaction rates increased as the carboxyl-to-hydroxyl ratios increased from 0.3 to 0.7. These increased reaction rates might have resulted in part from the increased probabilities of esterification reactions and their more volatile water byproducts, rather than the higher boiling EG yielded by the ester-interchange reactions, which were more prominent in samples with lower carboxyl-to-hydroxyl end-group ratios. In addition, the SSP of resins to a common final IV, from precursors of different IV_0 values, resulted in equivalent total end-group concentrations. The distribution of these end groups was different, however, with precursors exhibiting lower carboxyl-to-hydroxyl ratios and lower IV_0 values, yielding resins with corresponding reduced levels of carboxyl end groups.

SSP activation energies were calculated with rate constants obtained as functions of reaction times at polymerization temperatures of 160–230°C. These activation energies indicated the temperature dependence of the SSP controlling mechanisms. Changes in the reaction rates were seen most clearly for precursor A (IV = 0.50). As precursor IV increased from 0.50 to 0.64 dL/g, changes in the activation energies became less obvious. Possible SSP mechanisms have been proposed through comparisons of observed activation energies and literature values. Some phases of the SSP reaction process may include more than one rate-controlling mechanism, and the natures of these mechanisms appear to be influenced by the precursor IV and the reaction temperature.

At SSP reaction temperatures of 200–230°C, all three precursors displayed similar activation energies. The rate-determining mechanisms in this temperature range are thought to include the diffusion of chain end groups, acting together with the more widely acknowledged byproduct diffusion mechanism. In the lower temperature range (from 160 to 200°C), higher activation energies were required for all polymerizations; with the 0.50-IV precursor activation energy almost twice as high as those of the 0.56- and 0.64-IV precursors. In this lower temperature range, chemical reactions were the controlling mechanism for SSP of all three precursors. For the 0.50-IV material, end-group diffusion appeared to be an additional controlling mechanism.

The volume fraction levels of crystallinity, determined with a density gradient column, indicated that at each SSP temperature, samples prepared from precursors with lower IV_0's had higher levels of crystallinity. The changes in the crystallinity, obtained with DSC, were consistent with trends observed for the density results. In this case, samples prepared from the three precursors could be seen to fall into three distinct data sets. At each final resin IV, higher levels of crystallinity were present for samples prepared from lower IV precursors. The changes in the crystallite size, measured with a wide-angle X-ray diffraction technique, indicate that during SSP, the crystallite sizes increased quickly within the first few hours of the reaction and then stabilized. The crystallite sizes also increased with increasing SSP temperatures. The overall levels of crystallinity, as measured with techniques such as density and DSC, represented the total amounts of the crystalline phase present in PET. These values, determined at each SSP temperature, were controlled by the rates of crystallization, which were slightly increased for the precursors of lower molecular weights. The crystallite sizes, however, as determined with X-ray diffraction, were based on sizes of individual crystalline unit structures rather than the total numbers of these structures. The levels of crystallinity and the sizes of crystallites increased with increasing SSP temperatures, and both increased quickly during the initial stages of the SSP time, after which they remained relatively stable. The levels of crystallinity were slightly higher for equivalent samples prepared from lower molecular weight precursors, whereas the crystallite sizes did not systematically depend on the molecular weight.

Changes in the levels of the resin crystallinity are known to result in two competing changes in SSP reaction kinetics. A higher crystallinity tends to concentrate carboxyl and hydroxyl end groups in the amorphous phase of a partially crystalline polymer, as they are excluded from crystalline areas. This phenomenon is expected to increase the rate of the chemical reaction because more end groups are in close proximity to one another. At the same time, an opposing effect results from the reduced mobility and higher barrier characteristics provided by the crystalline phase. In this case, the increased crystallinity creates a path of greater tortuosity, making the longer diffusion path a greater obstacle to byproduct diffusion and thereby reducing the SSP reaction rate.

The authors thank the members of the PET Industrial Consortium who supported our research at the Polymer Institute of the University of Toledo.

References

1. Jabarin, S. In Polymeric Materials Encyclopedia; Salamone, J. C., Ed.; CRC: New York, 1996; Vol. 8, p 6078.
2. Ravindranath, K.; Mashelkar, R. Chem Eng Sci 1986, 41, 2197.
3. Huang, B.; Walsh, J. Polymer 1998, 39, 6991.
4. Gao, Q.; Huang, N.; Gerking, L. Chem Eng Sci 1997, 52, 371.
5. Ravindranath, K.; Mashelkar, R. J Appl Polym Sci 1990, 39, 1325.
6. Yuki, K. Saturated Polyester Resin Handbook; Nikkan Kougyosha: Tokyo, 1989; Chapters 2–4.
7. Groeninckx, G.; Reynaers, H.; Berghmans, H.; Smets, G. J Polym Sci Polym Phys Ed 1980, 18, 1311.
8. Groeninckx, G.; Reynaers, H. J Polym Sci Polym Phys Ed 1980, 18, 1325.
9. Leu, S.; McCarthy, A. Annu Tech Conf 1990, 1000.
10. Chen, S.; Chen, F. J Polym Sci Part A: Polym Chem 1987, 25, 533.
11. Mallon, F.; Ray, W. J Appl Polym Sci 1998, 69, 1233.
12. Devotta, I.; Mashelkar, R. Chem Eng Sci 1993, 10, 1859.
13. Wu, D.; Chen, F.; Li, R. Macromolecules 1997, 30, 6737.
14. Kang, C. J Appl Polym Sci 1998, 68, 837.
15. Chang, T. Polym Eng Sci 1970, 10, 364.
16. Jabarin, S.; Lofgren, E. J Appl Polym Sci 1986, 32, 5315.
17. Dröscher, M.; Wegner, G. Polymer 1978, 19, 43.
18. Zhang, H.; Rankin, A.; Ward, M. Polymer 1996, 37, 1079.
19. Zhang, H.; Ward, M. Macromolecules 1995, 28, 7622.
20. Al-Abdul-Razzak, S.; Lofgren, E.; Jabarin, S. Polym Int 2002, 51, 174.
21. Bunn, C.; Daubeny, R. Proc R Soc London Ser A 1954, 226, 531.
22. Fisher, E.; Fakirov, S. J Mater Sci 1976, 11, 1041.
23. Stouffer, J. M. (to E. I. du Pont de Nemours and Co.). U.S. Pat. 5,532,333 (1996).
24. Stouffer, J. M. (to E. I. du Pont de Nemours and Co.). U.S. Pat. 5,714,262 (1998).
25. Buxbaum, L. Angew Chem Int Ed Engl 1968, 7, 182.
26. Medellin-Rodriguez, F. J.; Lopez-Guillen, R.; Waldo-Mendoza, M. A. J Appl Polym Sci 2000, 75, 78.
27. Duh, B. J Appl Polym Sci 2002, 83, 1288.
28. Challa, G. Makromol Chem 1960, 38, 123.
29. Boudard, M. Kinetics of Chemical Processes; Prentice-Hall: Englewood Cliffs, NJ, 1968; Chapter 2.
30. Jabarin, S.; Lofgren, E. Polym Eng Sci 1984, 24, 1056.
31. Halek, G. J Polym Sci Polym Symp 1986, 74, 83.